SUPPORTING INFORMATION for:

Seizure-induced LTP in the dentate gyrus is pro-convulsant

Kaoutsar Nasrallah, M. Agustina Frechou, Young J. Yoon, Subrina Persaud, J. Tiago Gonçalves and Pablo E. Castillo

Corresponding authors: Pablo E. Castillo, MD/PhD and Kaoutsar Nasrallah, PhD

Email: pablo.castillo@einsteinmed.edu (lead contact)

kaoutsar.n@gmail.com

This PDF file includes:
SI Materials and Methods
Figures S1 to S11

SUPPLEMENTARY MATERIALS AND METHODS

Experimental Model and Subject Details

C57BL/6, *Bdnf* floxed (*Bdnf*$^{fl/fl}$) or *Drd2*-cre (B6.FVB(Cg)-Tg(Drd2-cre)ER44Gsat/Mmucd, MMRRC 032108-UCD) mice (2-3.5–month-old, both males and females) were used in this study. All animals were group housed in a standard 12 hr light/12 hr dark cycle and had free access to food and water. Animal handling, breeding and use followed a protocol approved by the Animal Care and Use Committee of Albert Einstein College of Medicine, in accordance with the National Institutes of Health guidelines. *Bdnf*$^{fl/fl}$ mice, generated by Dr. Jaenisch, were kindly donated by Dr. Lisa Monteggia (formerly at University of Texas, Southwestern Medical Center).

Acute hippocampal slice preparation

Acute transverse hippocampal slices (300 µm thick) were prepared from C57BL/6, *Bdnf*$^{fl/fl}$ and *Drd2*-cre mice. Animals were anesthetized with isoflurane and euthanized in accordance with institutional regulations. The hippocampi were then removed and cut using a VT1200s Microslicer (Leica Microsystems Co.) in a solution containing (in mM): 93 N-methyl-D-glucamine (NMDG), 2.5 KCl, 1.25 NaH_2PO_4, 30 $NaHCO_3$, 20 HEPES, 25 D-glucose, 2 Thiourea, 5 Na-Ascorbate, 3 Na-Pyruvate, 0.5 $CaCl_2$, 10 $MgCl_2$, 93 HCl. These slices were then transferred to 32°C extracellular artificial cerebrospinal fluid (ACSF) solution, containing (in mM): 124 NaCl, 2.5 KCl, 26 $NaHCO_3$, 1 NaH_2PO_4, 2.5 $CaCl_2$, 1.3 $MgSO_4$ and 10 D-glucose, for 30 min and then kept at room temperature for at least 40 min before recording. All solutions were equilibrated with 95% O_2 and 5% CO_2 (pH 7.4).

Electrophysiology

All recordings were performed at 28 ± 1°C in a submersion-type recording chamber perfused at 2 ml/min with ACSF. $GABA_A$ and $GABA_B$ receptor antagonists, picrotoxin (100 µM) and CGP55845 hydrochloride (3 µM), were included in the extracellular solution (ACSF) except in the experiments shown in Fig S1 and 11. Whole-cell patch-clamp recordings using a Multiclamp 700A amplifier (Molecular Devices) were made from GCs (in the upper blade of the DG) and MCs (Fig S1 and 11) voltage clamped at −60 mV (V_h = −60 mV, unless otherwise stated) using patch-type pipette electrodes (~3-4 MΩ) containing (in mM): 135 $KMeSO_4$, 5 KCl, 1 $CaCl_2$, 5 NaOH, 10 HEPES, 5 MgATP, 0.4 Na_3GTP, 5 EGTA and 10 D-glucose, pH 7.2 (288-291 mOsm). Series resistance (~6-25 MΩ for GCs and ~17-21 MΩ for MCs) was monitored throughout all experiments with a −5 mV, 80 ms voltage step, and cells that exhibited a significant change in series resistance (> 20%) were excluded from analysis. A cesium-based internal solution containing (in mM): 131 cesium gluconate, 8 NaCl, 1 $CaCl_2$, 10 EGTA, 10 D-glucose and 10 HEPES, pH 7.2 (289-295 mOsm), was used for the experiments shown in Fig S3. AMPA/NMDA ratio shown in Fig S3D, were calculated as AMPA EPSC amplitude/NMDA EPSC amplitude. AMPA EPSCs were recorded at V_h = −70 mV in presence of picrotoxin (100 µM) and NMDA EPSCs were collected at V_h = +40 mV in the same cell in presence of picrotoxin (100 µM) and after bath application of AMPA antagonist NBQX (10 µM). Experiments shown in Fig S1A-C were performed in current clamp mode. Mature GCs were identified by characteristic hyperpolarized membrane potential (checked immediately after membrane break in, -72 to -83 mV). Cells with high membrane resistance (> 800 MΩ) were considered as putative adult born GCs (1) and were excluded from the analysis. To activate MC axons, a broken tip (~10–20 µm) stimulating patch-type micropipette filled with ACSF was placed in the IML (< 50 µm from the border of the GC body layer) and paired,

monopolar square-wave voltage or current pulses (100 µs pulse width, 4-30 V) were delivered through a stimulus isolator (Digitimer DS2A-MKII). Typically, stimulation intensity was adjusted to obtain comparable magnitude of synaptic responses across experiments, e.g., 30-80 pA EPSCs (V_h = −60 mV), except for input/output experiments shown in Fig 3B, 4B-D, S3B, S5B, S6B-C and S10. MC-GC LTP was typically induced by 5 stimuli at 100 Hz repeated 50 times, every 0.5 s, except in Fig 6 (see below). Light evoked EPSCs (o-EPSCs), shown in Fig 6 C-E, were triggered using 1 ms pulses of blue light, provided by a collimated LED (Thorlabs, M470L3-C5, 470 nm, 300mW) and delivered through the microscope objective (40X, 0.8 NA). Recordings were performed in acute hippocampal slices < 700 µm from the optic fiber implant. The light was centered in the IML, and the light intensity adjusted to obtain ~60–120 pA responses (V_h = −60 mV). In the experiments shown in Fig 6C, LTP was induced using light stimulation of MC axons with the following protocol: 5 pulses of 1 ms, at 30 Hz repeated 50 times, every 0.5 s. In Fig S11, GC-MC synaptic strength was monitored. MCs identity was confirmed by the presence of a characteristic high frequency of spontaneous EPSCs, and by checking the firing pattern in response to depolarizing step of currents (non-burst firing and action potentials with almost no afterhyperpolarization) (2). GC axons were electrically stimulated in the DG subgranular zone using a bipolar theta glass ACSF-filled pipette. The mGluR2/3 agonist DCG-IV (1 µM), which selectively reduces GC-MC synaptic transmission (3, 4) was applied at the end of each experiment to confirm the nature of the stimulated input. To mimic physiological conditions, EPSCs were recorded in absence of GABA receptor blockers. Reagents were bath applied following dilution into ACSF from stock solutions stored at −20°C prepared in water or DMSO, depending on the manufacturer's recommendation.

Bdnf conditional KO

Bdnf$^{fl/fl}$ mice were injected with Cre expressing (AAV5-CaMKII-Cre-mCherry, 5.8 x10^{12} Virus Molecules/mL, UNC Vector) or control (AAV5-CaMKII-mCherry, 4.9 x10^{12} Virus Molecules/mL, UNC Vector) adeno-associated viruses. For electrophysiological experiments shown in Fig 4, Fig S4-6 and S9-10, 0.5 µl of virus was injected (flow rate of 0.1 µl/min) unilaterally into the dorsal blade of the DG (relative to bregma: 2.06 mm posterior, 1.5 mm lateral, 1.8 mm ventral) of 5-8–week-old (w.o.) *Bdnf*$^{fl/fl}$ mice. Slices for electrophysiology were prepared from injected animals, 2 to 4 weeks after injection. In postsynaptic cKO animals, we verified the absence of mCherry in the hilus of the whole ipsilateral hippocampus, as previously described (5). For seizure monitoring (Fig 5), BDNF mRNA labeling (Fig S7) and c-Fos labeling (Fig S8) experiments, 0.5 µl of virus was injected (flow rate of 0.1 µl/min) bilaterally into both the dorsal (relative to bregma: 1.9 mm posterior, 1.25 mm lateral, 2.1 mm ventral) and ventral (relative to bregma: 3.2 mm posterior, 2.2 mm lateral, 2.8 mm ventral) DG of 5-8–w.o. *Bdnf*$^{fl/fl}$ mice, and seizures were induced and monitored 2-3 weeks post-injection. Animals were placed in a stereotaxic frame and anesthetized with isoflurane (up to 5% for induction and 1%–3% for maintenance). In all experiments, both male and female mice were used with a similar ratio for the two types of viruses.

MC silencing

To silence MCs, the Gi inhibitory DREADD (iDREADD) was selectively expressed in MCs. The Cre-dependent AAV-CaMKII-DIO-hM4D(G_i)-mCherry (4.16 x 10^{13} vg/mL, prepared at Janelia Research Campus) or AAV-CaMKII-DIO-mCherry (control, 5.95 x10^{13} vg/mL, prepared at Janelia Research Campus) was injected (0.5 µl/site, at 0.1 µl/min) bilaterally into both the dorsal (relative to bregma: 1.9 mm posterior, 1.25 mm lateral, 2.1 mm ventral) and ventral (relative to bregma: 3.2 mm posterior, 2.2 mm lateral, 2.8 mm ventral) DG of 5-8–w.o. *Drd2*-Cre mice. Seizures were induced and monitored 2-3 weeks post-injection. The DREADD selective agonist clozapine-N-oxide (CNO, TOCRIS) was bath applied in acute slices in experiments shown in Fig 1D and S1. CNO was administered intraperitoneally in Fig 1E-H (2 mg/kg diluted in saline solution containing

2% DMSO) 30 min before *in vivo* seizure induction (KA IP), based on kinetics of CNO plasma levels and *in vivo* effects (6, 7). Viral expression was verified *posthoc*.

In vivo induction of MC-GC LTP with optogenetics

To induce MC-GC LTP *in vivo* by light-activating MCs, ChiEF was selectively expressed in MCs, and an optic fiber (200 µm diameter) was implanted unilaterally (relative to bregma: 1.9 mm posterior, 1.25 mm lateral, 1.8 mm ventral) to deliver blue light above the IML of the DG. The Cre-dependent AAV-hSyn-Flex-ChIEF-Tdtomato (2.4 $x10^{12}$ Virus Molecules/mL) was injected bilaterally (0.5 µl/site, at 0.1 µl/min) into both the dorsal (relative to bregma: 1.9 mm posterior, 1.25 mm lateral, 2.1 mm ventral) and ventral (relative to bregma: 3.2 mm posterior, 2.2 mm lateral, 2.8 mm ventral) DG of 5-8–w.o. *Drd2*-Cre mice. 5-7 weeks after surgery, MC-GC LTP induction protocol (5) was applied *in vivo*, by delivering a brief burst of blue light (5 pulses of 5 ms at 30 Hz, repeated 50 times every 0.5 s), using a fiber-coupled 470 nm LED light source (Thorlabs, MF470F3, ~7 mW output from the 200 µm optic fiber). Viral expression and optic fiber implant location were confirmed *posthoc*.

Seizure induction and monitoring

Seizures were induced acutely using intraperitoneal (IP) injection of 20-30 mg/kg of kainic acid (KA, HelloBio HB0355), prepared in saline solution the same day, in 2-3–month-old mice. To be able to see potential decrease and increase in seizure severity/susceptibility, 30 mg/kg (Fig 1, 2 and 5) and 20 mg/kg (Fig 6) of KA were used, respectively. Of note, seizures were less severe in *Drd2*-Cre mice as compared to C57BL/6 (wild type) and $Bdnf^{fl/fl}$ animals, likely due to strain differences (8). For MC-GC basal transmission and synaptic plasticity analysis, acute hippocampal slices were prepared when the animal reached stage 3 of convulsive seizures, i.e., forelimb clonus and rearing (Fig 3, S3, S4, S6 and S10) or 25 min post KA IP injections (Fig 4 and S5). Saline-injected mice were used as a control. For behavioral seizure scoring, mice were monitored during 120 min post-injection and behavioral seizures were scored, by an experimenter blind to condition (control *vs Bdnf* cKO or control *vs* MC silencing), using a modified Racine scale (9) as follows: stage 0: normal behavior, stage 1: immobility and rigidity, stage 2: head bobbing, stage 3: forelimb clonus and rearing, stage 4: continuous rearing and falling, stage 5: clonic-tonic seizure, stage 6: death. The maximum Racine score was recorded every 10 minutes and the cumulative seizure score was obtained by summing these scores across all 12 bins of the 120 min experiment. Mouse movements were visualized with an infrared camera for 2P imaging experiments (see below). For MC silencing experiments, IP injection of CNO (2 mg/kg, I.P) was delivered 30 min before inducing seizures with 30 mg/kg KA IP injection to both groups, control and inhibitory DREADD. For in vivo optogenetic experiments, LTP was induced 50 min before KA IP injection, and animals receiving sham-light stimulation were used as control.

Immunolabeling and posthoc confirmation of AAV expression

Two hours after KA (20-30 mg/kg in saline) intraperitoneal injection, mice were deeply anesthetized using isoflurane (3-5%) and transcardially perfused with 4% paraformaldehyde (PFA) in 0.1 M sodium phosphate buffer (PBS). After 24-48h fixation in 4% PFA, 50 µm-thick brain coronal sections were prepared using a DSK Microslicer (DTK-1000). Brain slices were washed in PBS (3 x 10 min) and then incubated for 2h at room temperature in a blocking solution containing 10% goat serum, 1% Triton X-100 in PBS. Primary antibody was applied for 24 h, at 4°C (rabbit anti-c-Fos, 1:1000; Cell Signaling, cat # 2250S, 0.1% Triton X-100, 5% goat in PBS). After 4 washes of 10 min in PBS, the sections were incubated with AlexaFluor 488-conjugated goat anti-rabbit (1:500, Invitrogen, cat # A11008) for 2 h at room temperature. Slices were washed twice in PBS for 10 min each, stained with 40,6-diamidino-2-phenylindole (DAPI, 1:1000 in PBS, 20 min, ThermoFisher) to label cell nuclei and mounted with Prolong diamond antifade reagent mountant (ThermoFisher) onto microscope slides. In Fig S2, the primary antibodies were applied

for 48 h, at 4°C [rabbit anti-glutamate receptor 2/3 (GluR2/3, 1:50; EMD Millipore, cat # AB1506) and mouse anti-GAD67 (1:500; EMD Millipore, cat # MAB5406) in 0.1% Triton X-100, 5% goat in PBS]. After 4 washes of 10 min in PBS, the sections were incubated with AlexaFluor 488-conjugated goat anti-rabbit (1:500, Invitrogen, cat # A11008) and AlexaFluor 647-conjugated goat anti-mouse (1:1000, Invitrogen, cat # A32728) for 2 hours at room temperature.

Fluorescent in situ hybridization in brain slices

Mice were deeply anesthetized using isoflurane (3-5%) and transcardially perfused with 4% PFA. 24-48h post-fixation in 4% PFA, 50 µm-thick brain coronal sections were prepared using a DSK Microslicer (DTK-1000). Fluorescent in situ hybridization (FISH) was performed using ViewRNA ISH Cell Assay kit (Thermo Fisher; QVC0001) following the manufacturer's instructions with a few modifications. The protease digestion step was omitted as it did not affect the labeling of the FISH probes. Permeabilization step was performed using the detergent solution provided in the kit with the duration extended to 15 minutes. The incubation time with the gene-specific probe set was increased to overnight to enhance labeling in tissue. All probe labeling steps were performed at 40 °C and the other remaining steps were performed at room temperature (RT). A gene-specific mouse BDNF probe set (VB6-15253-06) which recognizes all twelve splice variants was used to detect BDNF mRNA. In brief, the slices were washed in PBS and permeabilized at RT. The labeling of gene-specific probe was performed overnight. Subsequently, the pre-amplifier, amplifier, fluorescent label probes and DAPI labeling was performed the next day. The slices were mounted onto slides using Prolong Gold Antifade (Molecular Probes) and imaged using a confocal microscope.

Image Acquisition and cell quantification

Images were acquired using a Zeiss LSM 880 Airyscan Confocal microscope with Super-Resolution and ZEN (black edition) software and a 25X oil-immersion objective. All images were analyzed using Fiji and cells were counted using Cell Counter plug-in in Fiji, in the upper and lower blade of the DG in areas of maximum viral expression (> 70% of mCherry+ neurons), by an experimenter blind to the conditions. All infected cells were confirmed by using the DAPI channel, and individual counts were taken for c-Fos-expressing neuron to provide a percentage of c-Fos+ and mCherry^{+} cells among the total number of neurons identified using DAPI. For each animal, we used 1 dorsal and 1 ventral section. Right and left hippocampus were randomly used.

Adeno-Associated Virus Vector Construction

For the construction of AAV plasmids, the human Synapsin (hSyn) promoter in pAAV-hSyn-DIO-hM4D(Gi)-mCherry (Addgene, cat #: 50459) was replaced with mouse CaMKIIa promoter using MluI and SalI restriction sites to produce pAAV-CaMKII-DIO-hM4D(Gi)-mCherry and pAAV-CaMKII-DIO-mCherry. The AAVs were prepared at Janelia Research Campus.

Data analysis

Electrophysiological data were acquired at 5 kHz, filtered at 2.4 kHz, and analyzed using a Multiclamp 700A amplifier (Molecular Devices) and custom-made software for IgorPro 7.01 (Wavemetrics Inc.). PPR was defined as the ratio of the amplitude of the second EPSC (baseline taken 1-2 ms before the stimulus artifact) to the amplitude of the first EPSC. The interval between first and second EPSC was 100 ms. CV was calculated as the standard deviation of EPSC amplitude divided by mean EPSC amplitude. For each experiment, an average of 30 consecutive PPRs and CVs were used. The magnitude of LTP was determined by comparing 10 min baseline responses with responses 20-30 min after induction protocol. Averaged traces include 20 consecutive individual responses (or 5 consecutive responses for input/output experiments in Fig 3B, 4B-D, S3B, S4C, S6B-C and S10).

In vivo 2-photon imaging

WT mice (6-8–w.o.) were injected in the right dorsal hippocampus (relative to bregma: 1.2 mm posterior, 1.6 mm lateral, 1.9 mm ventral) with a viral vector encoding for the red-shifted Ca^{2+} sensor jRGECO1a [AAVDJ-CaMKIIa::NES-jRGECO1a-WPRE-SV40 (AAV-CaMKII-jRGECO1a), 950µL at 5.4 $x10^{12}$ viral particles/mL, University of North Carolina Vector Core, plasmid kindly donated by Dr. Fred Gage]. A 3-mm diameter craniotomy was drilled around the injection site 24 hrs after viral injection (10), the meninges, cortex, and corpus callosum were removed by aspiration and the hippocampus and alveus fibers were left intact. The lesion was irrigated with sterile saline throughout the procedure. A titanium window (3-mm diameter, 1.3-mm deep) with a glass bottom was implanted above the hippocampus. The implant was secured using dental cement and a titanium bar (34 × 4 × 1.3 mm) was attached to head-fix the mice to the microscope set-up. *In vivo* calcium imaging was performed 3-4 weeks after surgery, using a two-photon microscope (Thorlabs Bergamo) equipped with a 16x 0.8NA objective (Nikon) and a Fidelity-2 1070 nm laser (Coherent). The mice were head-fixed and placed on a 120 cm long treadmill belt. For optimum light transmission the angle of the mouse's head was adjusted to ensure that the imaging window was parallel to the objective. Movies of Ca^{2+} activity were acquired at 15 frames/s using an average laser power of ~180 mW, as measured in front of the objective. Stage 3 convulsive seizures (forelimb clonus) were identified using an infra-red camera. Raw calcium movies were registered to correct for motion artifacts using NoRMCorre (11). The regions of interest (ROIs) corresponding to individual cells were selected using Cellpose (12). These ROIs were manually curated to select granule and mossy cells, the fluorescence traces extracted using Fiji/ImageJ (13), and further analyzed with custom written algorithms (Python and MATLAB). For KA-injected mice, the mean fluorescence was determined for 500 frames selected around the plateau of a behavioral seizure (as determined by the observation of forelimb clonus, *Fseizure*), for each cell. For baseline activity, 500 frames were selected before the onset of the same behavioral seizure ($Fbaseline_{KA}$). For control groups, frame selection was performed similarly before ($Fbaseline_{sal}$) and after saline injection (*Fsaline*), matching the timeline of KA injected mice. ΔF/F was calculated as follows for both groups, for each cell:

$$\mathrm{Ca^{2+}\ signal_{seizure}} = \frac{Fseizure - Fbaseline_{KA}}{Fbaseline}$$

$$\mathrm{Ca^{2+}\ signal_{saline}} = \frac{Fsaline - Fbaseline_{sal}}{Fbaseline}$$

The timing of the onset of seizure activity was determined by detecting the changepoint of individual Ca^{2+} traces [MATLAB *findchangepts* function (14)].

Quantification and Statistical Analysis

The normality of all distributions was assessed using the Shapiro-Wilk test. In normal distributions, Student's unpaired and paired two-tailed t tests were used to assess between-group and within-group differences, respectively. The non-parametric paired sample Wilcoxon signed rank test and Mann-Whitney's U test were used in non-normal distributions. Statistical comparison in Fig 1F, 3B, 4B-D, 5C, 6G, S1C, S3B, S5B, S6B-C and S10 was performed using two-way ANOVA with repeated measure (RM) and Greenhouse-Geiser was used for correction of degrees of freedom when sphericity was not assumed. To compare differences in the magnitude of calcium activity waves between KA and saline injected mice, we used the R statistical analysis software to fit a generalized linear mixed effects model to ΔF/F for each individual MC and GC (Fig 2 E,F), using treatment as a fixed effect, and including animal identity as a random effect in order to account for differences between individual animals. P values were then calculated with an ANOVA test comparing our model to a null model with no treatment information and identical random effects.

Statistical significance was set to $p < 0.05$ ($***$ indicates $p < 0.001$, $**$ indicates $p < 0.01$, and $*$ indicates $p < 0.05$, n.s. indicates non-significant). All values are reported as the mean ± SEM. Experiments shown in Fig 1E-H, Fig 4, Fig 5, Fig S5 and Fig S7-8 were performed in blind manner during data acquisition and analysis. Statistical analysis was performed using OriginPro (version b9.2.272) software (OriginLab).

All data reported in this paper will be shared by the lead contact upon request.

REFERENCES

1. C. Schmidt-Hieber, P. Jonas, J. Bischofberger, Enhanced synaptic plasticity in newly generated granule cells of the adult hippocampus. *Nature* **429**, 184-187 (2004).
2. P. Larimer, B. W. Strowbridge, Nonrandom local circuits in the dentate gyrus. *J Neurosci* **28**, 12212-12223 (2008).
3. M. Lysetskiy, C. Foldy, I. Soltesz, Long- and short-term plasticity at mossy fiber synapses on mossy cells in the rat dentate gyrus. *Hippocampus* **15**, 691-696 (2005).
4. T. P. Hedrick *et al.*, Excitatory Synaptic Input to Hilar Mossy Cells under Basal and Hyperexcitable Conditions. *eNeuro* **4** (2017).
5. Y. Hashimotodani *et al.*, LTP at Hilar Mossy Cell-Dentate Granule Cell Synapses Modulates Dentate Gyrus Output by Increasing Excitation/Inhibition Balance. *Neuron* **95**, 928-943 e923 (2017).
6. D. F. Manvich *et al.*, The DREADD agonist clozapine N-oxide (CNO) is reverse-metabolized to clozapine and produces clozapine-like interoceptive stimulus effects in rats and mice. *Sci Rep* **8**, 3840 (2018).
7. P. D. Whissell, S. Tohyama, L. J. Martin, The Use of DREADDs to Deconstruct Behavior. *Front Genet* **7**, 70 (2016).
8. E. Rusina, C. Bernard, A. Williamson, The Kainic Acid Models of Temporal Lobe Epilepsy. *eNeuro* **8** (2021).
9. R. J. Racine, Modification of seizure activity by electrical stimulation. II. Motor seizure. *Electroencephalogr Clin Neurophysiol* **32**, 281-294 (1972).
10. A. Mizrahi, J. C. Crowley, E. Shtoyerman, L. C. Katz, High-resolution in vivo imaging of hippocampal dendrites and spines. *J Neurosci* **24**, 3147-3151 (2004).
11. E. A. Pnevmatikakis, A. Giovannucci, NoRMCorre: An online algorithm for piecewise rigid motion correction of calcium imaging data. *J Neurosci Methods* **291**, 83-94 (2017).
12. C. Stringer, T. Wang, M. Michaelos, M. Pachitariu, Cellpose: a generalist algorithm for cellular segmentation. *Nat Methods* **18**, 100-106 (2021).
13. J. Schindelin *et al.*, Fiji: an open-source platform for biological-image analysis. *Nat Methods* **9**, 676-682 (2012).
14. K. Haynes, P. Fearnhead, I. A. Eckley, A computationally efficient nonparametric approach for changepoint detection. *Stat Comput* **27**, 1293-1305 (2017).

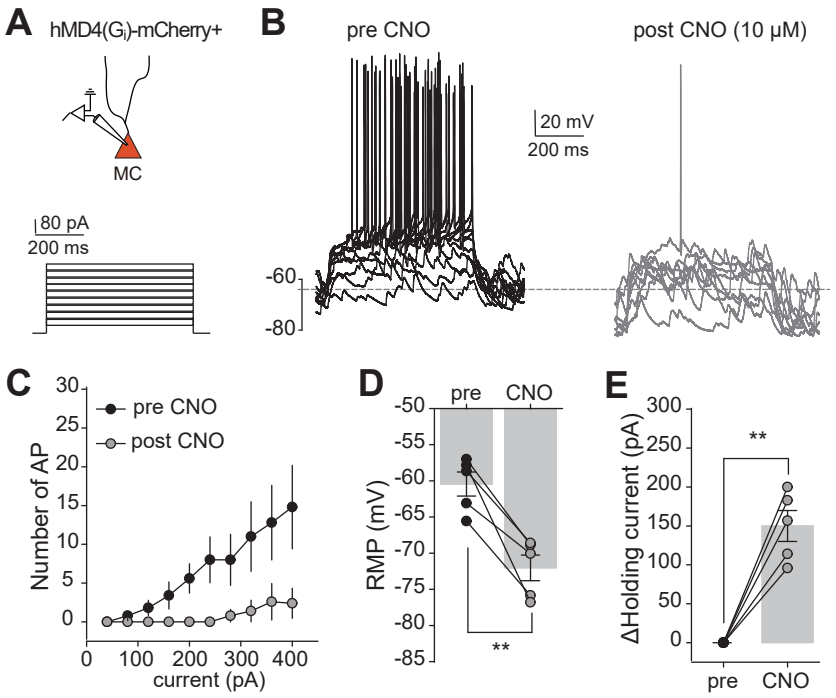

Figure S1: CNO inhibited iDREADD-expressing MC activity

(A) Whole-cell, voltage and current clamp recordings of iDREADD-mCherry-expressing MCs were obtained from*Drd2* -cre mice injected with AAV-CaMKII-DIO-hMD4(G_i)-mCherry.
(B) Voltage responses elicited by depolarizing current steps injection (from 40 pA to 400 pA , every 20 pA) from a single cell experiment before (left, black) and after (grey, right) bath application of CNO (10 µM). Horizontal line shows resting membrane potential (RMP) before CNO.
(C-E) Summary plots showing how CNO (10 µM) reduced (C) the number of action potential (AP, pre vs post CNO: p = 0.0029, n = 5, Bonferroni post-test pairwise comparison) and (D) resting membrane potential (RMP, pre vs CNO: p = 0.004, n = 5, paired t-test), while it increased (E) holding current (pre vs CNO: p = 0.002, n = 5, paired t-test).
** p < 0.01. Data are presented as mean ± SEM

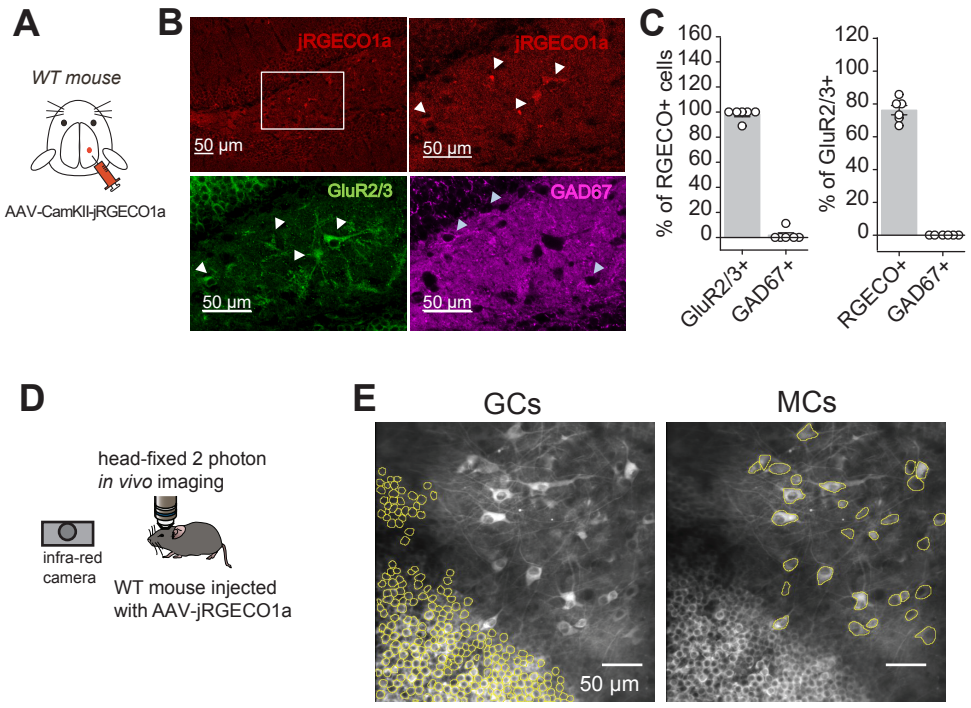

Figure S2: jRGECO1a-expressing neurons in the DG

(A) AAV-CaMKII-jRGECO1a was unilaterally injected into the dorsal DG of WT mice.
(B) jRGECO1a was selectively expressed in MCs in the hilus of AAV-CamKII-jRGECO1a-injected mice. Confocal images of jRGECO1a expression (red) in the DG (top). High-magnification images of the hilus showing that jRGECO1a-expressing hilar neurons (red, top right) are MCs (white arrowheads) identified with GluR2/3$^+$ immunostaining (green, bottom left). Bottom right, hilar interneurons identified with GAD67$^+$ immunostaining (magenta, blue arrowheads) are not infected with jRGECO1a.
(C) Specificity (left, 98.15 ± 1.88 % of jRGECO1a$^+$ neurons are GluR2/3$^+$, n = 6 slices, N= 3 mice) and extend (right, 76.2 ± 2.8 % of GluR2/3$^+$ expressed jRGECO1a$^+$, n = 6 slices, N= 3 mice) of jRGECO1a expression.
(D) Diagram showing jRGECO1a-expressing MCs and GCs imaged in head-fixed mice monitored with IR camera.
(E) Example of mean image of jRGECO1a-expressing MCs (hilus) and GCs (granule cell layer) obtained during KA-induced convulsions, illustrating ROIs corresponding to individual GCs (left) and MCs (right).

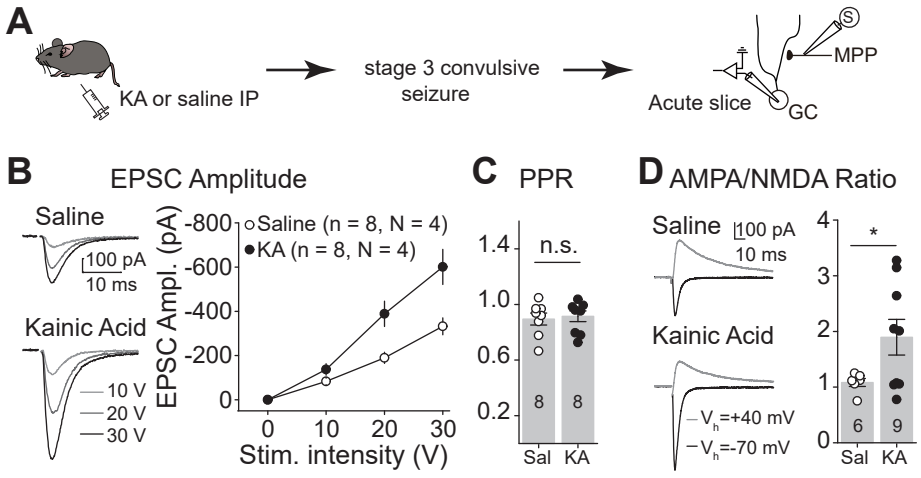

Figure S3: KA-induced seizure increased MPP-GC synaptic strength likely via a postsynaptic mechanism

(A) Seizures were acutely induced using KA IP (20 mg/kg). Mice were sacrificed once stage 3 of convulsive seizures was reached and MPP-GC synaptic function was accessed in acute hippocampal slices. Saline-injected mice were used as control.
(B) Representative traces and summary plot showing increased input/output function in KA-injected mice (two-way ANOVA RM, IP injection: $F(1, 7) = 10.52$, $p = 0.014$, stimulation intensity: $F(1.21, 8.46) = 64.44$, $p < 0.0001$; IP injection x stimulation intensity: $F(1,7) = 89.25$, $p < 0.0001$).
(C, D) No significant change in PPR (C) was detected ($p = 0.73$, unpaired t-test) while the AMPA/NMDA ratio was significantly increased (D) in KA-injected mice as compared to controls ($p = 0.036$, unpaired t-test)
* $p < 0.05$, n.s. $p > 0.05$. Data are presented as mean ± SEM.

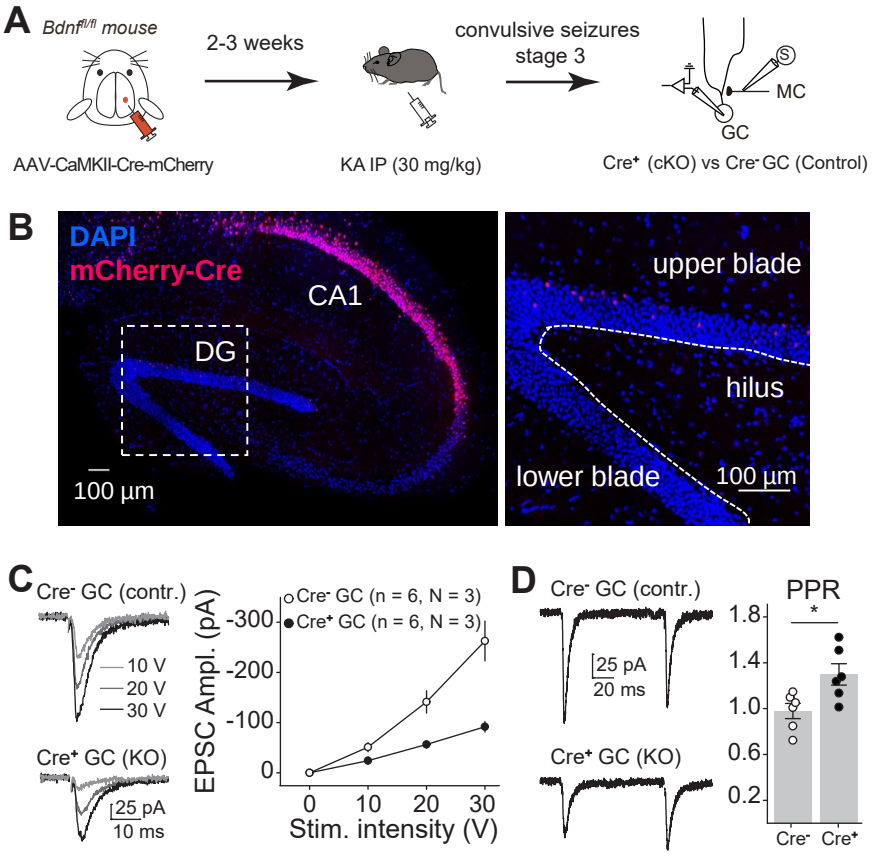

Figure S4: Genetic removal of *Bdnf* from GCs significantly reduced KA-induced MC-GC synaptic strengthening

(A) Experimental timeline. Cre-expressing AAV (AAV-CaMKII-Cre-mCherry) was injected unilaterally into the DG dorsal blade *of Bdnf*$^{fl/fl}$ mice. Experimental seizures were induced 2-3 weeks later using KA IP (30 mg/kg) and acute hippocampal slices were prepared at stage 3 of convulsive seizures. Whole cell recordings were obtained from Cre-mCherry$^+$ and Cre-mCherry$^-$ GCs, in response to MC axon stimulation.
(B) Single plan confocal images showing the expression of Cre-mCherry in the granule cell layer of the upper but not the lower blade of the DG. Note the absence of AAV in the hilus.
(C) Traces and summary plot showing how KA-induced increase in EPSC amplitude was significantly impaired in Cre$^+$ as compared to Cre$^-$ GCs (two-way ANOVA RM, Cre$^+$ vs Cre$^-$: $F(1, 5) = 19.52$, $p = 0.007$, stimulation intensity: $F(1.03, 5.15) = 40.85$, $p = 0.0012$; Cre x stimulation intensity: $F(1,5) = 87.41$, $p = 0.0002$).
(D) PPR was significantly increased in *Bdnf*-lacking GCs (Cre$^+$) as compared to Cre$^-$ neighboring GCs ($p = 0.019$, unpaired t-test).
* $p < 0.05$. Data are presented as mean ± SEM.

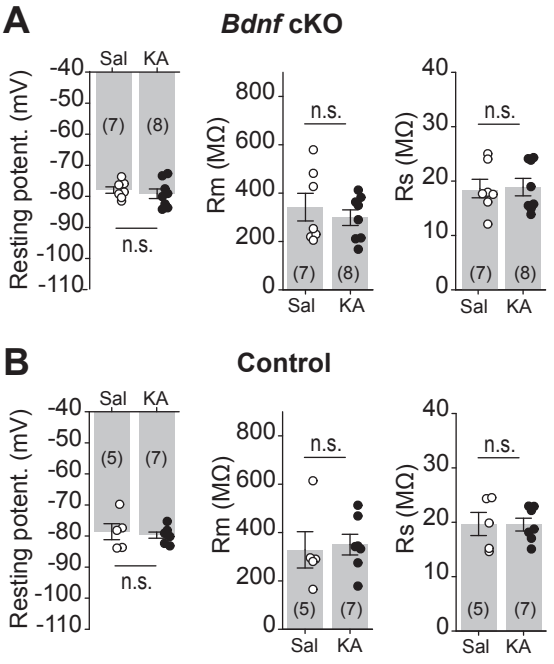

Figure S5: *Bdnf* cKO did not alter GC membrane properties

(A) *Bdnf* $^{fl/fl}$ mice were injected with Cre-expressing virus (AAV-CaMKII-Cre-mCherry, *B dnf* cKO). Whole cell recordings were performed in Cre-mCherry-expressing GCs. Resting potential (saline: -77.3 ± 1.0 mV, n = 7; KA: -79.2 ± 1.6 mV, n = 8; saline vs KA: $p > 0.05$, unpaired t-test), membrane resistance (Rm, saline: 340.9 ± 57.0 MΩ, n = 7; KA: 298.5 ± 32.9 MΩ, n = 8; saline vs KA: $p > 0.05$, unpaired t-test) and series resistance (Rs, saline: 18.3 ± 1.7 MΩ, n = 7; KA: 18.9 ± 1.6 MΩ, n = 8; saline vs KA: $p > 0.05$, unpaired t-test) were not different in KA (30 mg/kg) vs saline-treated.
(B) *Bdnf* $^{fl/fl}$ mice were injected with a control virus (AAV-CaMKII-mCherry). Membrane properties were similar in KA- and saline-injected mice (Resting potential, saline: -78.6 ± 2.6 mV, n = 5; KA: -79.7 ± 1.0 mV, n = 7; saline vs KA: $p > 0.05$, unpaired t-test; Rm, saline: 328.7 ± 75.2 MΩ, n = 5; KA: 350.2± 42.5 MΩ, n = 7; saline vs KA: $p > 0.05$, Mann Whitney test; Rs, saline: 19.7 ± 2.1 MΩ, n = 5; KA: 19.6± 1.8 MΩ, n = 7; saline vs KA: $p > 0.05$, unpaired t-test).

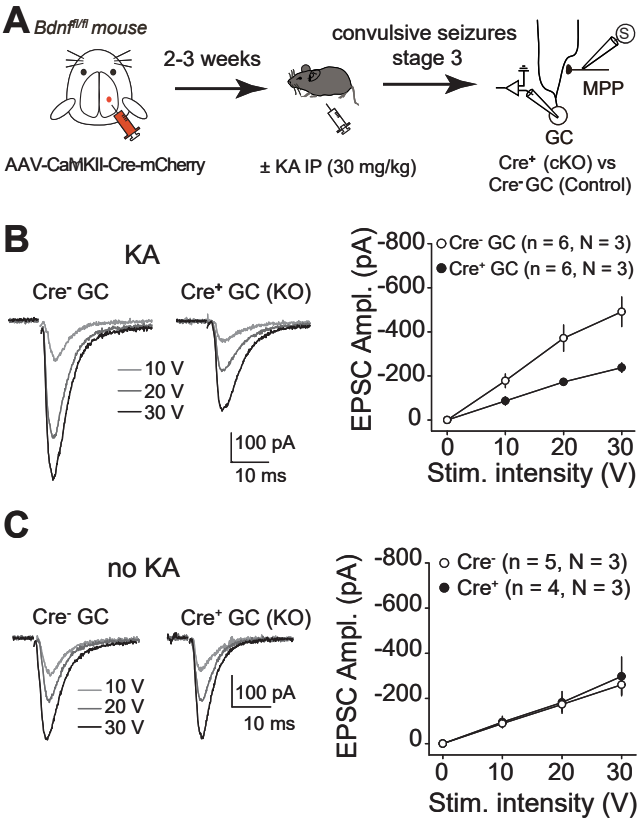

Figure S6: *Bdnf* genetic removal from GCs significantly reduced KA-induced MPP-GC synaptic strengthening

(A) Cre-expressing AAV (AAV-CaMKII-Cre-mCherry) was injected unilaterally into the DG dorsal blade of *Bdnf*$^{fl/fl}$ mice. Seizures were induced 2-3 weeks later using KA IP (30 mg/kg) and acute hippocampal slices were prepared at stage 3 of convulsive seizures. Whole-cell recordings of Cre-mCherry^{+} vs Cre-mCherry^{-} GCs were performed and MPP axons were electrically stimulated.
(B) Traces and summary plot showing that the KA-induced increase in EPSC amplitude was significantly impaired in Cre^{+} GCs (*Bdnf* cKO) as compared to Cre^{-} GCs (two-way ANOVA RM, Cre^{+} vs Cre^{-}: $F(1, 5) = 14.31$, $p = 0.013$, stimulation intensity: $F(1.28, 6.41) = 27.87$, $p = 0.0011$; Cre x stimulation intensity: $F(1,5) = 107.9$, $p = 0.00014$).
(C) Representative traces and summary plots showing that *Bdnf* genetic removal from GCs did not trigger any significant change in MPP-evoked EPSC amplitude in absence of KA IP injection (two-way ANOVA RM, Cre^{+} vs Cre^{-}: $F(1, 3) = 0.68$, $p = 0.47$, stimulation intensity: $F(1.06, 3.17) = 13.74$, $p = 0.03$; Cre x stimulation intensity: $F(1,3) = 17.04$, $p = 0.026$).
Data are presented as mean ± SEM.

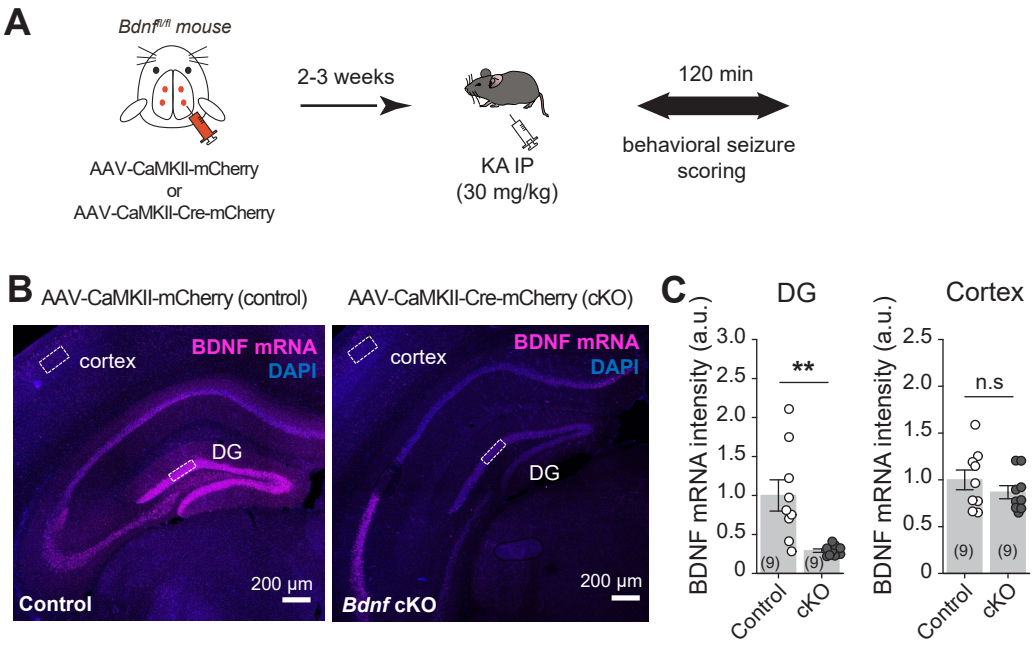

Figure S7: Injection of AAV-CaMKII-Cre-mCherry into the hippocampus of *Bdnf*$^{fl/fl}$ mice strongly reduced *Bdnf* mRNA levels

(A) AAV-CaMKII-mCherry (control) or AAV-CaMKII-Cre-mCherry (cKO) was injected bilaterally into ventral and dorsal DG of *Bdnf*$^{fl/fl}$ mice.
(B, C) Confocal images (B) and summary plots (C) showing that the *Bdnf* mRNA fluorescent signal was largely and significantly reduced in the DG of *Bdnf* cKO animals as compared to controls (p = 0.008, unpaired t-test; n = 9 slices/condition from N = 3 mice/condition). Note that no significant change in *Bdnf* mRNA levels was detected outside of the hippocampus (cortex: p = 0.31, unpaired t-test, n = 9 slices/ condition from N = 3 mice/condition).
** p < 0.01, n.s. p > 0.05. Data are presented as mean ± SEM.

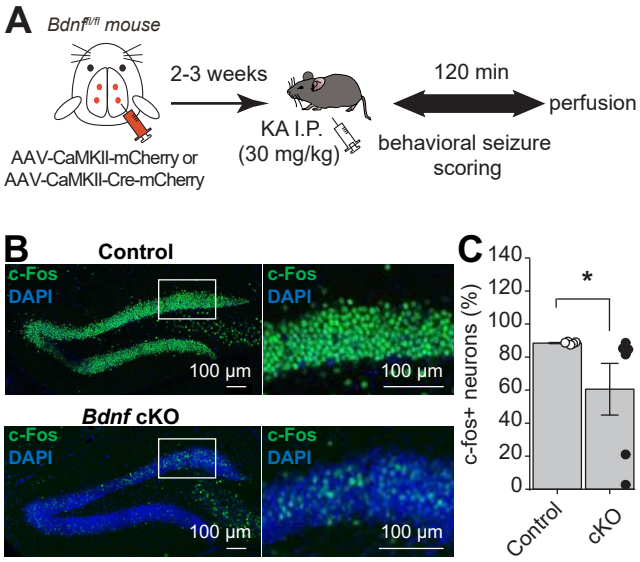

Figure S8: Neuronal *Bdnf* deletion reduced c-Fos expression in the DG of KA-injected mice

(A) Diagram of the experimental timeline.
(B, C) Confocal images (B) and quantification (C) showing that *Bdnf* KO reduced the number of c-Fos⁺ neurons in the DG of KA-injected mice (control: 88.5 ± 0.3% of c-Fos⁺ neurons, N = 5 mice; *Bdnf* cKO: 60.5 ± 15.6% of c-Fos⁺ neurons, N = 6 mice; control vs *Bdnf* cKO: $p < 0.05$, Mann Whitney test).

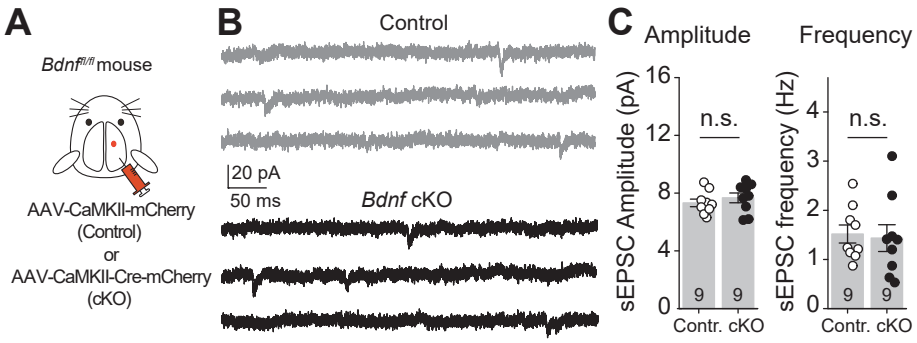

Figure S9: *Bdnf* cKO did not affect sEPSCs in GCs

(A) AAV-CaMKII-mCherry (control) or AAV-CaMKII-Cre-mCherry (cKO) was injected unilaterally into the DG of *Bdnf*$^{fl/fl}$ mice.
(B, C) Representative traces and summary plots showing that both sEPSC amplitude ($p = 0.80$, unpaired t-test) and frequency ($p = 0.43$, unpaired t-test) were similar in control and *Bdnf*-lacking GCs.
n.s. $p > 0.05$. Data are presented as mean ± SEM.

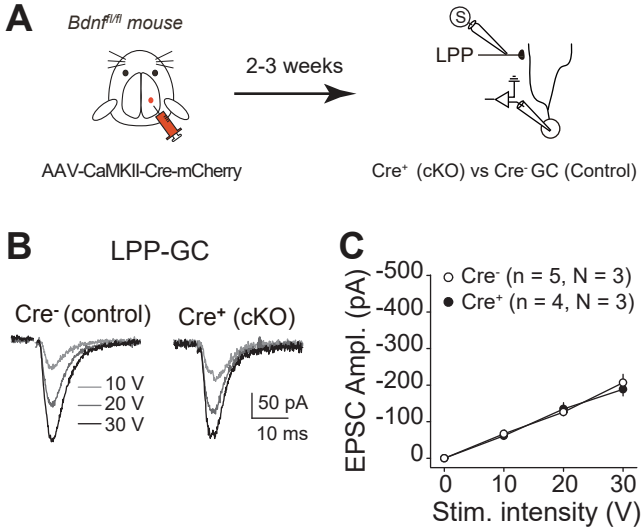

Figure S10: *Bdnf* cKO did not alter basal entorhinal cortex - GC excitatory transmission

(A) AAV-CaMKII-Cre-mCherry (cKO) was unilaterally injected into DG of *Bdnf*$^{fl/fl}$ mice. Whole cell recordings were performed in Cre^{+} (*Bdnf* cKO) vs Cre^{-} (control) GCs in response to MPP or LPP stimulation.
(B, C) LPP-evoked EPSC showed similar amplitude in Cre^{+} (*Bdnf* cKO) as compared to Cre^{-} (control) GCs (two-way ANOVA RM, Cre^{+} vs Cre^{-}: $F(1, 3) = 0.56$, $p = 0.51$, stimulation intensity: $F(1.12, 3.36) = 132.89$, $p = 0.0008$; Cre x stimulation intensity: $F(1,3) = 362.64$, $p = 0.0003$).
Data are presented as mean ± SEM.

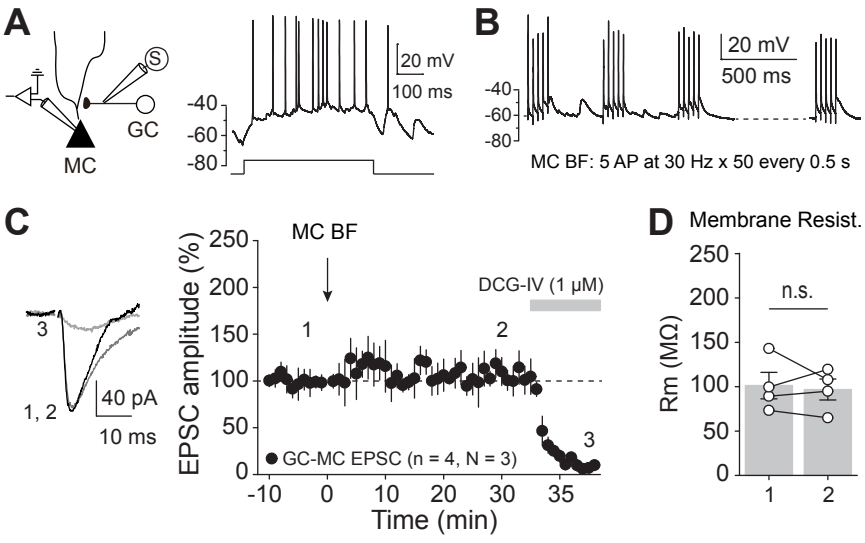

Figure S11: MC Burst Firing did not induce long-term changes at GC-MC synapse

(A) Left, diagram showing the recording configuration. Whole-cell recordings were performed in MCs in response to GC axon stimulation, while both excitatory and inhibitory transmission were left intact. Right, voltage response elicited by a depolarizing current step injection (shown below, 200-400 pA) illustrating typical MC firing pattern.
(B) Current-clamp recordings showing the induction protocol. MC Burst Firing (MC BF) was composed of 5 AP at 30 Hz, repeated 50 times, every 0.5 s.
(C) Representative traces and time course summary plot showing that application of MC BF did not induce any significant long-term change of GC-MC EPSC amplitude (105.9 ± 10.7 % of baseline, n = 4, p > 0.05, paired t-test). DCG-IV was applied at the end of each experiment to confirm the GC input nature.
(D) MC membrane resistance was not affected by MC BF application (before MC BS: 101.3 ± 14.9 MΩ, after MC BS: 96.8 ± 11.8 MΩ, before *vs* after MC BS: p > 0.05, paired t-test, n = 4).